

Effects of stress reduction on geomechanical and acoustic relationship of overconsolidated sands

Sirikarn Narongsirikul^{1,3*}, Nazmul Haque Mondol^{1,2} and Jens Jahren¹

¹Department of Geosciences, University of Oslo, Problemveien 7, 0315, Oslo, Norway, ²Norwegian Geotechnical Institute (NGI), Oslo, Norway, and ³ConocoPhillips Norway, Ekofiskvegen 35, 4056, Tananger, Norway

Received April 2019, revision accepted October 2019

ABSTRACT

Relationship between different geomechanical and acoustic properties measured from seven laboratory-tested unconsolidated natural sands with different mineralogical compositions and textures were presented. The samples were compacted in the uniaxial strain configuration from 0.5 to 30 MPa effective stress. Each sand sample was subjected to three loading–unloading cycles to study the influence of stress reduction. Geomechanical, elastic and acoustic parameters are different between normal compaction and overconsolidation (unloaded and reloaded). Stress path (K_0) data differ between normal consolidated and overconsolidated sediments. The K_0 value of approximately 0.5 is founded for most of the normal consolidated sands, but varies during unloading depending on mineral compositions and textural differences. The K_0 and overconsolidation ratio relation can be further simplified and can be influenced by the material compositions. K_0 can be used to estimate horizontal stress for drilling applications. The relationship between acoustic velocity and geomechanical is also found to be different between loading and unloading conditions. The static moduli of the overconsolidated sands are much higher than normal consolidated sands as the deformation is small (small strain). The correlation between dynamic and static elastic moduli is stronger for an overconsolidation stage than for a normal consolidation stage. The results of this study can contribute to geomechanical and acoustic dataset which can be applied for many seismic-geomechanics applications in shallow sands where mechanical compaction is the dominant mechanism.

Key words: Overconsolidation, Stress path, Static, Dynamic elastic.

1 INTRODUCTION

Effective stress reduction due to sediment uplift or excess pore fluid pressure affects acoustic, geomechanical and petrophysical properties (Holt 1990; Bowers and Katsube 2002; Zimmer *et al.* 2007; Narongsirikul, Mondol and Jahren 2019a,b). Increase of vertical weight on the sediments results in porosity loss, as well as increase of velocity and density in the underlain sediments. In a contrary, unloading the stress acting on rocks results in velocity and porosity reversal. However, the reversal of velocity and density is not fully re-

gained back the values as the previous stress level due to permanent deformation (Bower 1995; Bowers and Katsube 2002).

The different effects the stress condition has on the sediment properties, due to different burial histories, need to be considered in reservoir characterization and seismic modelling studies. Moreover, in the seismic-related geomechanics field, understanding the correlation between geomechanical parameters and acoustic relations is critical, as one data type (e.g. seismic velocities) can be used to extract another (e.g. mechanical stress and strain). A link between acoustic/seismic and geomechanical parameters can be expressed through various

*E-mail: Sirikarn_nar@hotmail.com

relationships. The relation between dynamic and static elastic moduli is one of the most common correlations in geomechanics. This relation is especially required when the dynamic moduli calculated from acoustic logs are needed to convert to static elastic moduli, as the static moduli are rarely obtained due to limited core measurements. The static elastic properties such as Young's and Shear Modulus, and Poisson's ratio, are important for geomechanical modelling. Uniaxial or constrained modulus is important for reservoir compaction study. Another common relationship is between velocity and strain. Previous studies have demonstrated that such a correlation is effective in evaluating seismic-geomechanics coupling via R-factor, a ratio of the change between velocity and in the vertical strain (e.g. Hatchell and Bourne 2005; Holt, Nes and Fjær 2005; Røste, Stovas and Landro 2005; Rickett *et al.* 2007; Herwanger and Horne 2009). This correlation means seismic responses of four-dimensional time-shift or time-strain can give information about geomechanical changes due to production, that is deformation and dilation. Another geomechanical parameters which are important for geomechanics applications are horizontal stresses. These parameters are often accurately obtained through leak off test or borehole breakout data. However, without drilling, the horizontal stresses need to be estimated by other means. Previous studies show that the stress path (K_0) can give an estimation of effective horizontal stress if effective vertical stress is known (Holt 1999; Grande, Mondol and Berre 2011; Holt *et al.* 2016). K_0 can also be estimated by overconsolidation ratio (OCR, Jaky 1948; Mayne and Kulhawy 1983).

The seismic and rock mechanical relations of normally compacted sediments have been investigated extensively through laboratory experiments on compacted sands studies (Yin 1992; Tao, King and Nabi-Bidhendi 1995; Dvorkin and Nur 1996; Chuhan *et al.* 2003; Pettersen 2007; Mondol *et al.* 2010; Fawad *et al.* 2011; Bhuiyan *et al.* 2013). Such experiments lead to a good collection of data that can be utilized for geomechanics and seismic integration for normal consolidation (NC) stress conditions. However, a few experimental approaches have been developed with the aim of understanding the effects of stress unloading on rock properties for overconsolidated (OC) sediments (Holt 1994; Nygård *et al.* 2004; Bhuiyan, Kolstø and Holt 2011; Grande *et al.* 2011; Dræge *et al.* 2014; Avseth and Lehocky 2016). More studies can mature the understanding of the subject and increase the collection of database for seismic and geomechanical applications such as reservoir compaction and time-lapse seismic studies.

This study reports an experimental investigation of seven unconsolidated sands with varying mineralogical compositions and textures, aiming at mechanical parameters obtained from the same laboratory measurements performed by Narongsirikul *et al.* (2019a). The study applies cyclical stress paths under zero horizontal strain conditions (K_0) including three stages of loading, partial unloading and reloading to investigate different behaviours between NC and OC. Mechanical properties (stress, strain, OCR and K_0) measured from the experiments are reported. These data are used to estimate static elastic moduli. The acoustic velocity data studied in Narongsirikul *et al.* (2019a,b) are used to estimate dynamic elastic properties. The relationships between rock acoustic and mechanical properties, and the different behaviours between normal compaction and OC are investigated. The study aims at correlating different geomechanical parameters together with acoustic and computed elastic properties, which are common for geomechanics and seismic applications.

2 NORMAL CONSOLIDATION VERSUS OVERCONSOLIDATION

Normal consolidation (NC) refers to a continuous stress increase during sediments compaction. NC, normal compaction, normal loading and virgin compaction are the terms used interchangeably. In contrast, sediments that are at present found at lower stress than previously experienced due to a reduction of the overburden (erosional unloading) or due to excess pore pressure are termed overconsolidated (OC; e.g. Pender 1978; Bjørlykke 2010). The term 'pre-consolidation stress' was used for the past maximum effective stress prior to stress reduction if the sediments have been preloaded. The overconsolidation ratio (OCR) is defined by the difference between past maximum effective vertical stress $\sigma'_{v \max}$ and the present effective vertical stress σ'_v , (Casagrande 1936) that is

$$\text{OCR} = \frac{\sigma'_{v \max}}{\sigma'_v}. \quad (1)$$

When the OCR is equal to 1, sediments are normally consolidated, that is when the past maximum effective stress and the present effective stress are equal.

K_0 can be used for an estimation of the effective horizontal stress as well as an indication of stress anisotropy. K_0 usually defined a stress path for the sediment loaded under a uniaxial strain condition in soil mechanics. K_0 is the ratio

between horizontal effective stress σ'_h and vertical effective stress σ'_v , that is

$$K_0 = \frac{\sigma'_h}{\sigma'_v}. \quad (2)$$

For example, for $K_0 = 1$, the stress is hydrostatic implying that the vertical and horizontal effective stresses are equal. For $K_0 < 1$, the stress is uniaxial and the vertical effective stress is greater than the horizontal effective stress. For loose sand sediments loaded under normal consolidation, K_0 equals approximately 0.5 (Grande *et al.* 2011).

Finally, the term effective stress, σ' , is defined as $\sigma' = \sigma - \alpha p$, where σ is the total stress, and subscript v and h denote the direction of vertical and horizontal stresses, respectively, p is the pore pressure and α is an effective stress coefficient. Following Terzaghi (1943), the effective stress coefficient value is assumed to be 1 for unconsolidated sediments.

3 STATIC AND DYNAMIC ELASTIC MODULI

Elastic moduli are elastic parameters which can be derived from laboratory measurement and well logs. The elastic moduli calculated from deformational experiments are the static moduli. Whilst, the elastic moduli calculated from elastic wave velocities (P- and S- waves, V_p and V_s) and density (ρ) are the dynamic moduli (Mavko, Mukerji and Dvorkin 2009). Five elastic parameters considered in the present study are listed below. The definition and the equation are based on Mavko *et al.* (2009).

Young's Modulus, E , for static is defined as the ratio of the extensional stress to the extensional strain in a uniaxial stress state:

$$E_{\text{static}} = \frac{\sigma_{zz}}{\varepsilon_{zz}}. \quad (3)$$

For dynamic:

$$E_{\text{dynamic}} = \rho V_s^2 \frac{(3V_p^2 - 4V_s^2)}{(V_p^2 - V_s^2)}. \quad (4)$$

Poisson's ratio, ν , for static is defined as minus the ratio of the lateral strain to the axial strain in a uniaxial stress state:

$$\nu_{\text{static}} = \frac{\sigma_{zz}}{\varepsilon_{zz}}. \quad (5)$$

For dynamic:

$$\nu_{\text{dynamic}} = \frac{(V_p^2 - 2V_s^2)}{2(V_p^2 - V_s^2)}. \quad (6)$$

Constrained or P-wave modulus, M , for static is defined as the ratio of the axial stress to the axial strain in a uniaxial strain state:

$$M_{\text{static}} = \frac{\sigma_{zz}}{\varepsilon_{zz}}. \quad (7)$$

For dynamic:

$$M_{\text{dynamic}} = \rho V_p^2. \quad (8)$$

Bulk Modulus, K , for static is defined as the ratio of the hydrostatic or isotropic stress, σ_0 , to the volumetric strain ($\varepsilon_{\alpha\alpha}$):

$$K_{\text{static}} = \frac{\sigma_0}{\varepsilon_{\alpha\alpha}}. \quad (9)$$

For dynamic:

$$K_{\text{dynamic}} = \rho \left(V_p^2 - \frac{4}{3} V_s^2 \right). \quad (10)$$

Shear Modulus, μ , for static is defined as the ratio of the shear stress to the shear strain. It can be defined by the functions between Young's Modulus (E) and Poisson's Ratio (ν) as

$$\mu_{\text{static}} = \frac{E}{2(1+\nu)}. \quad (11)$$

For dynamic:

$$\mu_{\text{dynamic}} = \rho V_s^2. \quad (12)$$

4 DATASET AND EXPERIMENTAL PROCEDURE

The same data as reported in Narongsirikul *et al.* (2019a) are used herein. A total of seven experimental compaction tests were performed on seven brine-saturated natural sand aggregates with varying mineral compositions and textures (Tables 1 and 2).

An axi-symmetric triaxial cell located at the Norwegian Geotechnical Institute was used for measurements of rock properties in this study. The samples were initially isotropically compacted to an effective stress of 0.52 MPa in the triaxial cell. The effective stress was then increased from 0.52 to 30 MPa under a uniaxial strain condition (K_0), which was maintained through adjustment of radial stress (σ'_h , onset, Fig. 1). Pore pressure was kept constant at 1 MPa throughout the experiments. To assure complete saturation prior to compaction, vacuum was applied before fluid saturation to ensure no air was left inside the samples. Carbon dioxide (CO_2) was then applied and left within the samples for a few minutes

Table 1 Mineral compositions from the XRD analysis (after Fawad *et al.* 2011)

Mineral constituents (weight percentage, %)						
Sample name	Quartz	Feldspar ¹	Clay ²	Other minerals ³	Effective grain density (g/cc)	Initial porosity (%)
Quartz arenite 1 (QA1)	95.27	4.73	–	–	2.65	36
Quartz arenite 2 (QA2)	97.88	1.77	–	0.35	2.65	41
Sub arkose 1 (SA1)	91.27	8.73	–	–	2.65	38
Sub arkose 2 (SA2)	77.19	22.81	–	–	2.64	34
Arkosis arenite (AA)	54.84	34.18	10.97	–	2.65	42
Volcanic arenite (VA)	4.84	52.51	–	42.65	2.81	40

¹Includes K-feldspar, albite, and plagioclase.

²Includes kaolinite and illite.

³Mostly present in volcanic arenite including aragonite, calcite, ankerite, amphibole and augite.

before brine solution (35 g NaCl per litre of water) was injected into the samples. Finally, the back pressure application was introduced to ensure fully liquid saturation. Details of the back pressure application can be found in Berre (2011). At 15, 25 and 30 MPa, effective stresses partial unloading was carried out by decreasing the vertical load followed by reloading to the next stress level (Fig. 1).

A maximum strain amplitude of the order of 10^{-2} can be achieved in this experiment setup. The strains were continuously recorded during each loading and unloading cycle through the changes in the sample height and diameter using vertical and horizontal deformation sensors (Fig. 1). Wave velocities both P- and S- and density data were taken from Narongsirikul *et al.* (2019a) to estimate the dynamic elastic properties of the sands. The detailed setup of the triaxial cell is described in detail in Berre (2011) and Narongsirikul *et al.* (2019a).

5 EXPERIMENTAL RESULTS

5.1 Stress, strain, K_0 and overconsolidation ratio

Figure 2 shows relations between (a) stress–strain (b) stress– K_0 (c) overconsolidated ratio (OCR)–strain and (d) OCR– K_0 for all sand samples at all pressure steps. Solid lines in all plots denote normal consolidation and dashed lines signify overconsolidation from unloading/reloading. OCR and K_0 are calculated using equations (1) and (2), respectively. The general observation for all the plots shows that all samples in an overconsolidated (OC) condition exhibit distinctive behaviour compared to the samples during normal compaction. The difference in magnitude of the parameters between the samples is attributed to the variations in the mineral compositions and textures of each sample.

Figure 2(a) shows the stress–strain relationship plotted for all samples. The stress versus strain relation is an important

coupled attribute for a reservoir during compaction, which is commonly known to result from production/injection-related stress changes. The slopes calculated from stress–strain relation yield the uniaxial compaction coefficient which is one of the key parameters for the estimation of the magnitude of reservoir deformation (Geertsma 1973). From the plot, strain increases with an increase in effective stress in the range 50–180 millistrain at the maximum effective stress at 30 MPa. In general, the samples with quartz rich content of >90% quartz content [quartz arenite 1 (QA1), quartz arenite 2 (QA2) and sub arkose 1 (SA1)] establish flatter slopes than the samples with medium to low quartz content [sub arkose 2 (SA2), arkosis arenite (AA) and feldspathic greywacke (FG), except volcanic arenite (VA)] during normal loading. The VA sample has the lowest quartz content. However, the sample exhibits intermediate stress–strain gradient between high and low quartz samples, instead of steep slope like what observed for other low quartz members. Other minerals (e.g. aragonite and calcite) of VA composite may contribute to this behaviour (See Table 2). At any given stress level, decreasing quartz content (increase of ductile and clay minerals) results in higher strain or compressibility. This shows that rock composition affects the compaction behaviour. However, this behaviour contrasts with that of the samples under unloading/reloading conditions, where different constituents do not significantly govern the degree of deformation, since all samples exhibit similar unloading strain–stress gradients (Fig. 2a). This may be due to the effect of permanent deformation the sands experienced from pre-stressing. The strain observed in all samples for OC curves shows elastic hysteresis. For all unloading cycles, the slopes of stress and strain curve (dashed lines) are of the same degree regardless of the change in the pre-consolidation stresses.

Figure 2(b) shows the stress– K_0 relation for all loading, unloading and reloading cycles. As reviewed in the

Table 2 Textural variations of the sand samples (after Fawad *et al.* 2011), sand grain size distribution (weight percentage, %), sorting classification and grain shapes (fraction)

Sample	Very coarse >1000 μm	Coarse 500–1000 μm	Med. 250–500 μm	Fine 125–250 μm	Very fine 63–125 μm	Silt <63 μm	Mean grain size (μm)	Sorting degree (ϕ)	Sorting Classification	Roundness (fraction)	Sphericity (fraction)
QA1	0.52	4.77	39.86	40.23	4.90	9.72	213.2	1.00	Poorly sorted	0.57	0.48
QA2	0.02	1.09	78.69	18.48	0.84	0.88	303.5	0.51	Moderately well sorted	0.54	0.42
SA1	4.66	32.32	61.80	1.19	-	0.03	466.5	0.60	Moderately well sorted	0.58	0.48
SA2	0.37	22.38	40.57	20.07	0.30	16.31	257.0	1.31	Poorly sorted	0.45	0.35
AA	0.02	4.09	58.49	28.76	1.04	7.60	250.0	0.90	Moderately sorted	0.47	0.38
VA	-	0.06	18.13	74.21	0.21	7.39	180.5	0.69	Moderately well sorted	0.53	0.43

introductory section, K_0 can be used to estimate the effective horizontal stress as well as an indicator of stress anisotropy. Here, we find that as the samples underwent normal compaction under a uniaxial strain condition, K_0 ranges between 0.45 and 0.55 (solid lines) and remains fairly constant across the stress range between 5 and 30 MPa. This observation is comparable with a typical K_0 value of 0.5 for unconsolidated sands under normal consolidation in soil mechanics. For normal consolidation, the difference in mineral compositions is responsible for variations in the K_0 development where the samples with high quartz content (>90% weight percent), that is QA2, QA1 and SA1 (black, magenta and blue solid lines) show high K_0 compared to samples with lower quartz contents (i.e. SA2, AA, VA and FG). Increasing amount of quartz (decreasing amount of clays and ductile minerals) increases K_0 . For OC when the stress was removed during the unloading with resultant decreasing effective stress, the development of K_0 increases approaching 1 (dashed lines). This means that the vertical and horizontal stress becomes less anisotropic from stress reduction.

Figure 2(c) illustrates the OCR–strain relation for all samples. The definition of the OCR is referred to in equation (1). During normal consolidation (NC), the OCR is equal to 1 (solid lines) as the maximum effective stress is the same as present effective stress. Therefore, the NC condition plots at OCR = 1 for all samples. When the samples were de-stressed and re-stressed, depicted by dashed lines, increasing the OCR does not change the strain significantly due to hysteresis effect (permanent damage of pore structure during preconsolidation). This behaviour is observed for all unloading cycles.

Figure 2(d) demonstrates the relation between OCR and K_0 . A clear separation can be observed between the normal compaction trend (solid lines plotted at OCR = 1) and OC lines (dashed lines). The unloading/reloading trends show linearly proportional relationship between OCR and K_0 where K_0 increases with an increase in the OCR. At the points where the OCR is equal to 1 and K_0 is equal approximately to 0.5, the samples are at the maximum effective stress prior to the stress reduction. As the stress was further reduced from the maximum stress point, the OCR and K_0 begin to increase in a linear fashion. As previously stated, that the K_0 can be an indicator of stress anisotropy, this means the reduction in the effective stress causes the stress anisotropy to become weaker as K_0 approaches 1 (isotropic).

In the same plot (Fig. 2d), we also find that the samples that comprised greater amounts of quartz exhibit higher K_0 at any given OCR. For example, at OCR 2.5, a group of samples that comprised high quartz (QA2, QA1, SA1) has

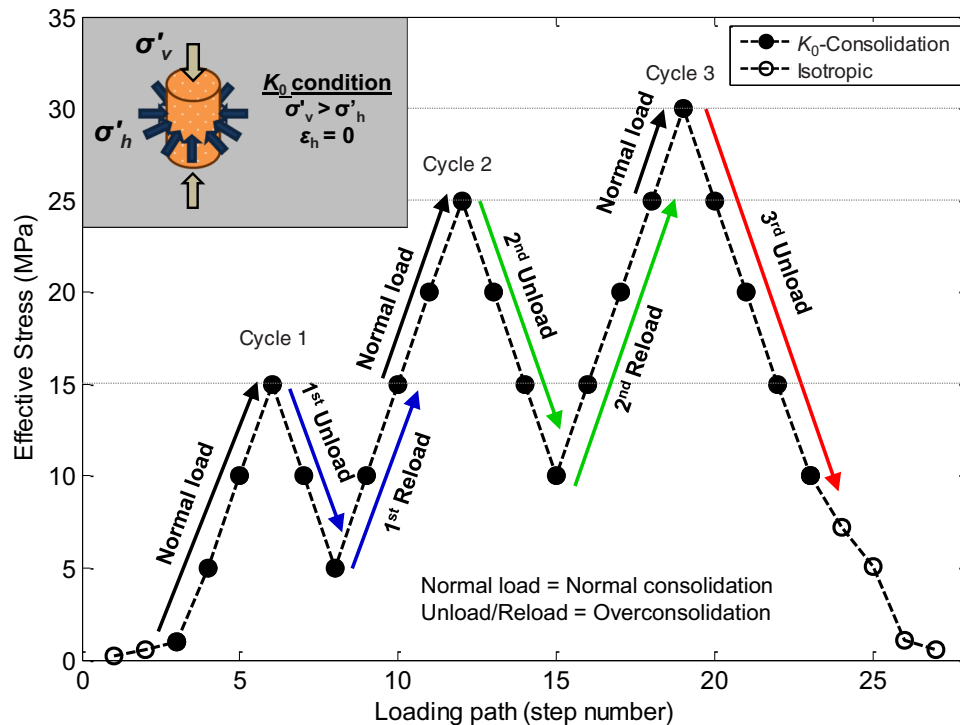


Figure 1 Loading protocol for experimental mechanical compaction applied to the sand samples in the present study (from Narongsirikul *et al.* 2019a). The procedure employs loading, unloading and reloading cycles. Unloading was applied at 15, 25 and 30 MPa effective stresses before further reloading. The uniaxial strain loading (K_0 -consolidation) condition is demonstrated in the upper left corner of the figure where zero horizontal strain, $\epsilon_h = 0$, is controlled by adjustment of effective horizontal stress, σ'_h , while the effective vertical stress is increased, σ'_v .

K_0 of approximately 0.85–0.9 while the group of samples with lower quartz (SA2, AA, FG, VA) has K_0 of 0.65–0.75. The SA2 sample has lower K_0 than what is expected from a sample with a moderate amount of quartz content. This may be explained by textural parameter differences, possibly the sorting in this sample may have a stronger control than the mineralogy alone.

5.2 Relationship between acoustic and mechanical properties

Measurements of the acoustic and mechanical properties of the samples expressed as relationships between strain versus velocities, K_0 versus velocities and overconsolidation ratio (OCR) versus velocities plots are shown in Fig. 3. The P-wave velocities are on the left column (Fig. 3a,c,e) and the S-wave velocities are on the right column (Fig. 3b,d,f). In general, all three mechanical properties exhibit similar relationships with P-wave and S-wave velocities. The difference is the magnitude where the shear wave propagation phenomenon is overall slower than the compressional wave. The normal consolidation (NC) trends (solid lines) are noticeably different

from the overconsolidation (OC) trends (OC, dashed lines). In addition, mineral compositions still play a significant role in exhibiting the relation varying between samples to samples in all plots.

In the strain–velocities plot (Fig. 3a,b), the inter-relation between these attributes are non-linear at low strain and later develop a linear trend at higher strain as the deformation continues. These behaviours are observed for all samples during normal compaction (solid lines). As with the strain–stress plot (Fig. 2), a significant deviation from normal compaction occurs for OC (dashed lines). The strain–velocity coefficient for OC is low compared to normal compaction, indicated by the low gradient on all unloading cycle lines. This means a small change in strain can be expected from a large change of velocities in overconsolidated sediments. In both OC and NC conditions, we find that the magnitude of strain changes correlate linearly with the changes in velocity. The link between these attributes can be useful approximation of the R-factor in seismic geomechanics application where R-factor is defined the ratio between travel time changes due to velocity changes and the path length changes due to physical strain changes (Hatchell and Bourne 2005; Røste *et al.* 2005). This

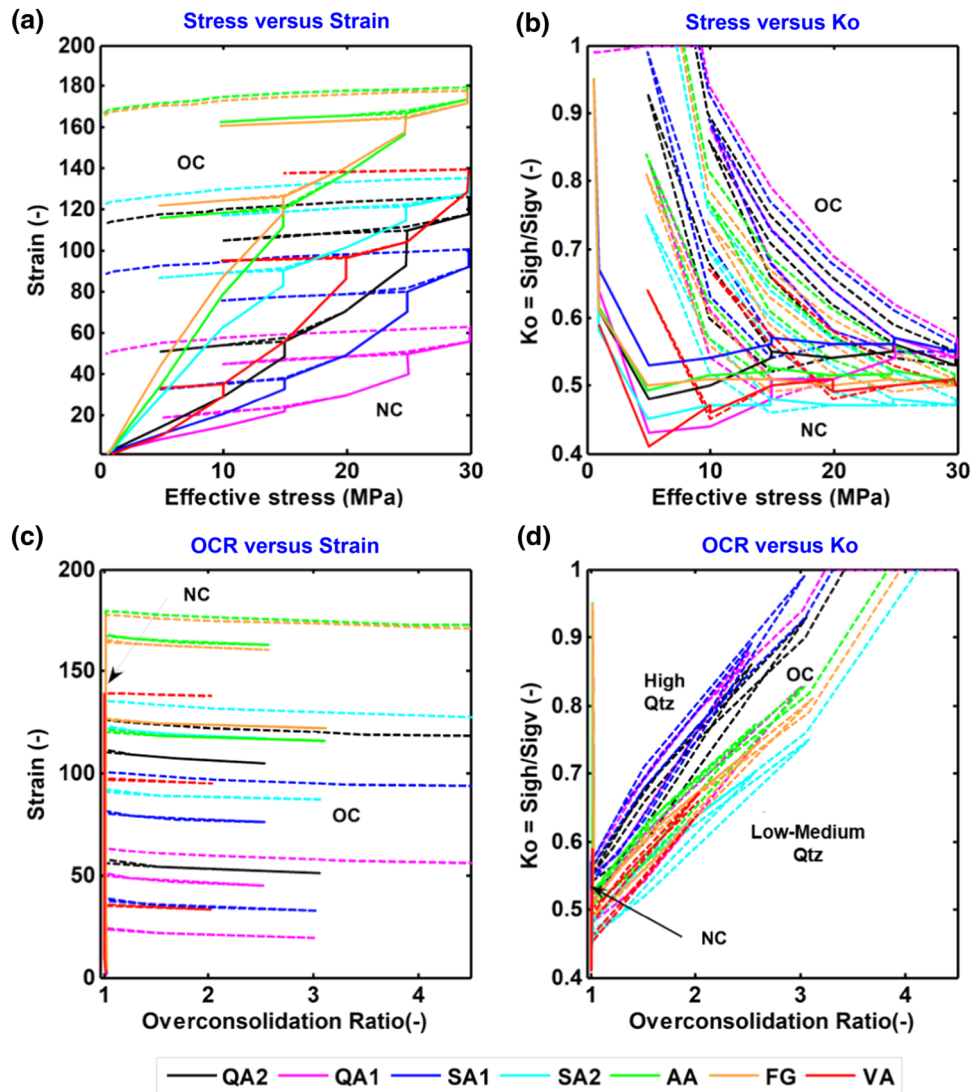


Figure 2 Geomechanical parameters for all samples and all loading/unloading/reloading cycles expressed in term of (a) stress and strain, (b) stress and K_0 , (c) Overconsolidation ratio (OCR) and strain and (d) OCR and K_0 . The normal consolidation trend (NC, solid lines, OCR = 1) separates clearly from overconsolidation trend (OC, dashed lines). The data span in all plots is attributed to the mineralogical and textural differences comprised in each sample.

R-factor allows the transformation from seismic travel-time to displacement.

In the K_0 and OCR versus velocities plot (Fig. 3c–f), an increase of either K_0 or OCR means the effective stress is decreased. As a consequence, the velocities for both P- and S-waves decrease from the maximum pre-consolidation stress (dashed lines). The K_0 and OCR versus velocities show the same behaviour both during NC where the values are constant and during OC where the value shows an inverted polynomial trend.

5.3 Dynamic and static moduli

Dynamic elastic moduli obtained by wave propagation measurements or log-derived data are a well-known application for seismic modelling studies. For example, fluid substitution required effective bulk and shear stiffness information. Static elastic moduli are of the same importance as this information is often used in many *in situ* stress applications, for example wellbore stability, compaction and hydraulic fracturing. In linear elasticity of isotropic homogenous materials, static elastic moduli or stiffness is generalized by Hooke's law, $\sigma = -C/\epsilon$,

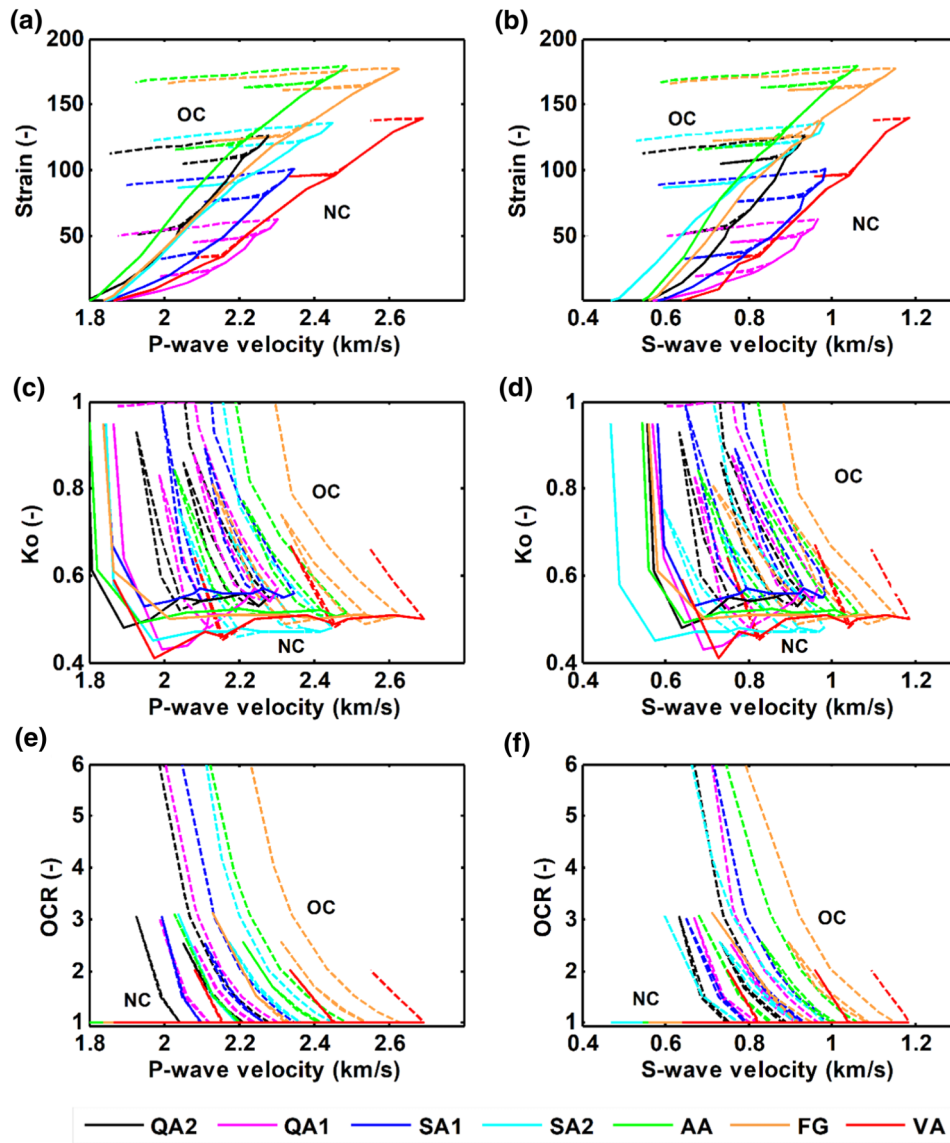


Figure 3 Geomechanical versus acoustic relations for all samples demonstrating links between velocities, both P- and S-waves, and, from the top down, strain (a, b), K_0 (c, d) and OCR (e, f), respectively. The normal consolidation (NC) stage is plotted as solid lines and overconsolidation (OC) stage is plotted as dashed lines. The NC and OC stages clearly have different trends.

where the modulus, C , is a ratio between stress, σ , and strain, ε . The static moduli are not often acquired due to expensive coring. Therefore, the conversion from commonly obtained dynamic moduli to static moduli is important. Figures 4–6 show the static and dynamic elastic parameters derived from experimental measurements in the present study. The equation and the description of the elastic moduli for each parameter, both static and dynamic, were explained in the Section 3. The parameters presented herein comprised constrained modulus, bulk modulus, shear modulus, Young’s modulus and Poisson’s Ratio.

In Fig. 4, measurement of static (open symbol) and dynamic (filled symbol) elastic parameters between the two end members, the quartz arenite 2 (QA2, red) and the feldspathic greywacke (FG, blue), were plotted. VA has the lowest quartz content. However, VA’s other composite minerals are uniquely different from other samples. Therefore, FG was used to represent the end member instead. Both the normal consolidated stages and unloading/reloading stages for all cycles are included in the plots and depicted as a circle symbol and a square symbol, respectively. All the static and dynamic properties were plotted as functions of effective stress. For

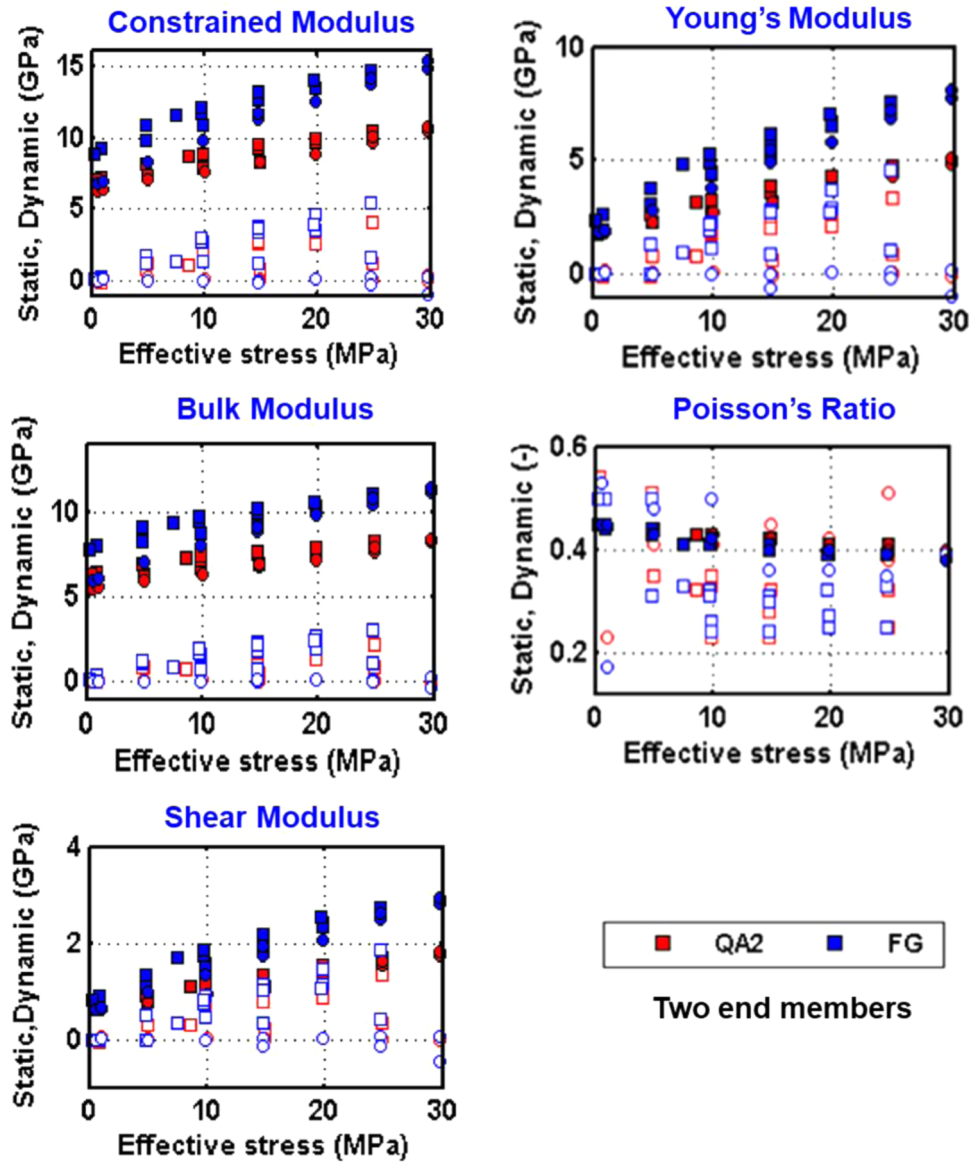


Figure 4 Elastic moduli parameters, both static (open symbols) and dynamic (filled symbols), versus effective stress for two representative samples, QA2 (red) and FG (blue). The plots are for all pressure steps both normal loading (circles) and unloading/reloading (square).

all the elastic parameters, dynamic moduli (fill symbol) overall are higher than static moduli (filled symbol) as expected. The quartz arenite 2 sample that represents the high quartz end member has lower elastic moduli than the low quartz feldspathic greywacke. However, the magnitude difference between the two end members is less pronounced for static elastic moduli.

All plots in Figs 5 and 6 show a relationship between static and dynamic elastic moduli for all samples at all pressure steps. Figure 5 colour-codes the data with effective stress

which is grouped into low, medium and high stress levels. Figure 6 colour-codes the data with quartz content separating into three groups of 0–40%, 40–80% and >80% quartz percentage. The red solid line in all plots is one-to-one correspondence (1:1 relationship) between the moduli. The black solid lines are the differences where the correspondences are one-to- n , where $n = 0.25, 0.5, 2, 4$ and 8 . The higher number of n shows the greater difference between the static and dynamic moduli. All derived data plot on the left side of the one-to-one correspondence indicate that the dynamic moduli are higher

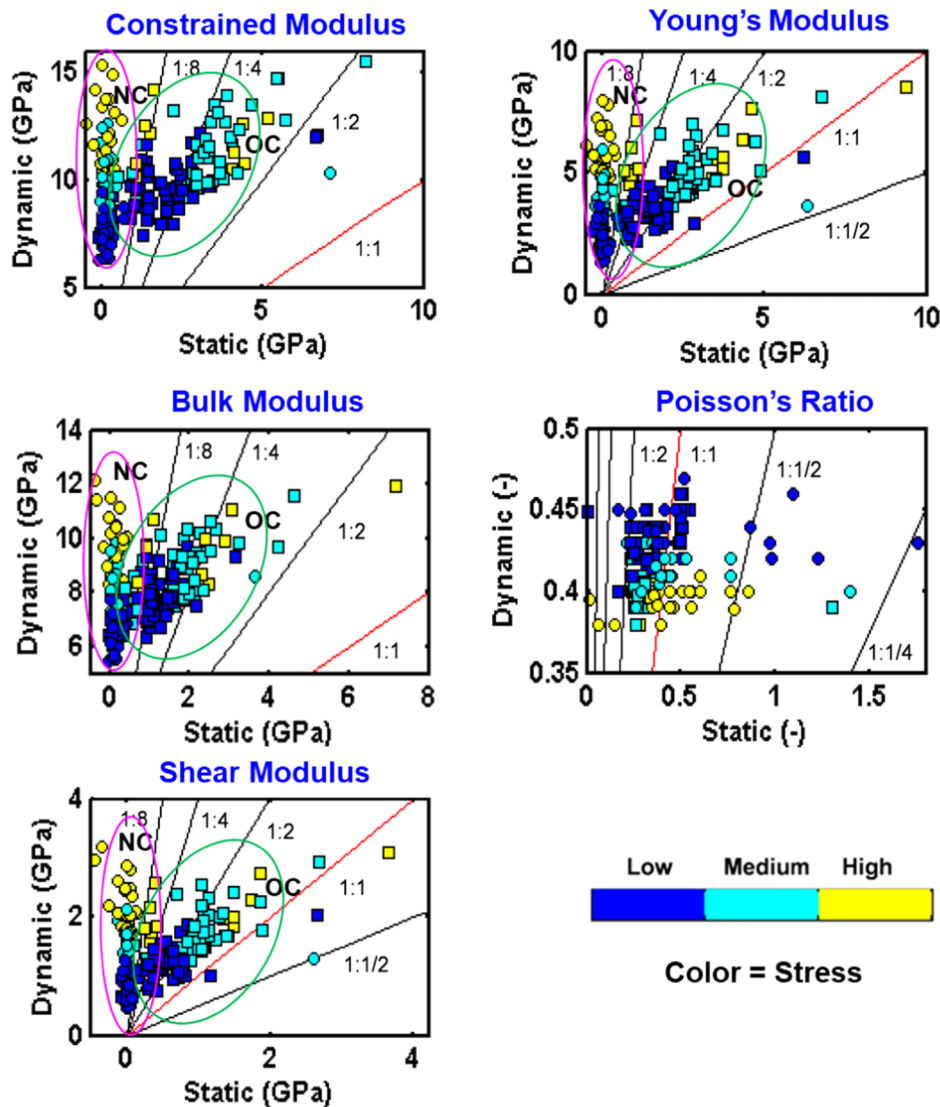


Figure 5 Relations between static and dynamic properties for all samples coloured by applied stress for all samples. Circles are normal consolidated (NC) sands, and squares are overconsolidated (OC) sands. The correspondences between 1:0.25 and 1:8 were projected on all static and dynamic elastic moduli relations. In all plots, for NC (circles) dynamic moduli are higher than static moduli and increase with stress as the data plotted beyond 1:8 correlation. The overconsolidated samples (squares) have static and dynamic elastic relationship closer to 1:1 correspondence.

than static moduli, except for Poisson's ratio where the data are plotted close to 1:1 relationship. Note that Poisson's ratio is the mechanical parameter that represents strain-strain relationship, instead of stress-strain relationship like the other four moduli. Therefore, the dynamic-static elastic relation can be different from the other elastic moduli.

The deformation during normal compaction is far greater than the deformation during unloading/reloading at any given stress. Therefore, the derived static elastic moduli for normal compaction data (circles) were expected to be low (due to

higher strain). This agrees with the observations for all elastic moduli in Figs 5 and 6 (circles) that the normal compaction data are plotted as very low values of static moduli, indicating that the sediments loaded under normal compaction are more compliant. The relation between static and dynamic elastic properties is very different, indicating by the observed data, is beyond the one-to-eight correspondence. In contrast, the static moduli of the overconsolidated (OC) sands are much higher as the deformation is small (small strain). Therefore, the static moduli are high and the rock is stiff due to the effect

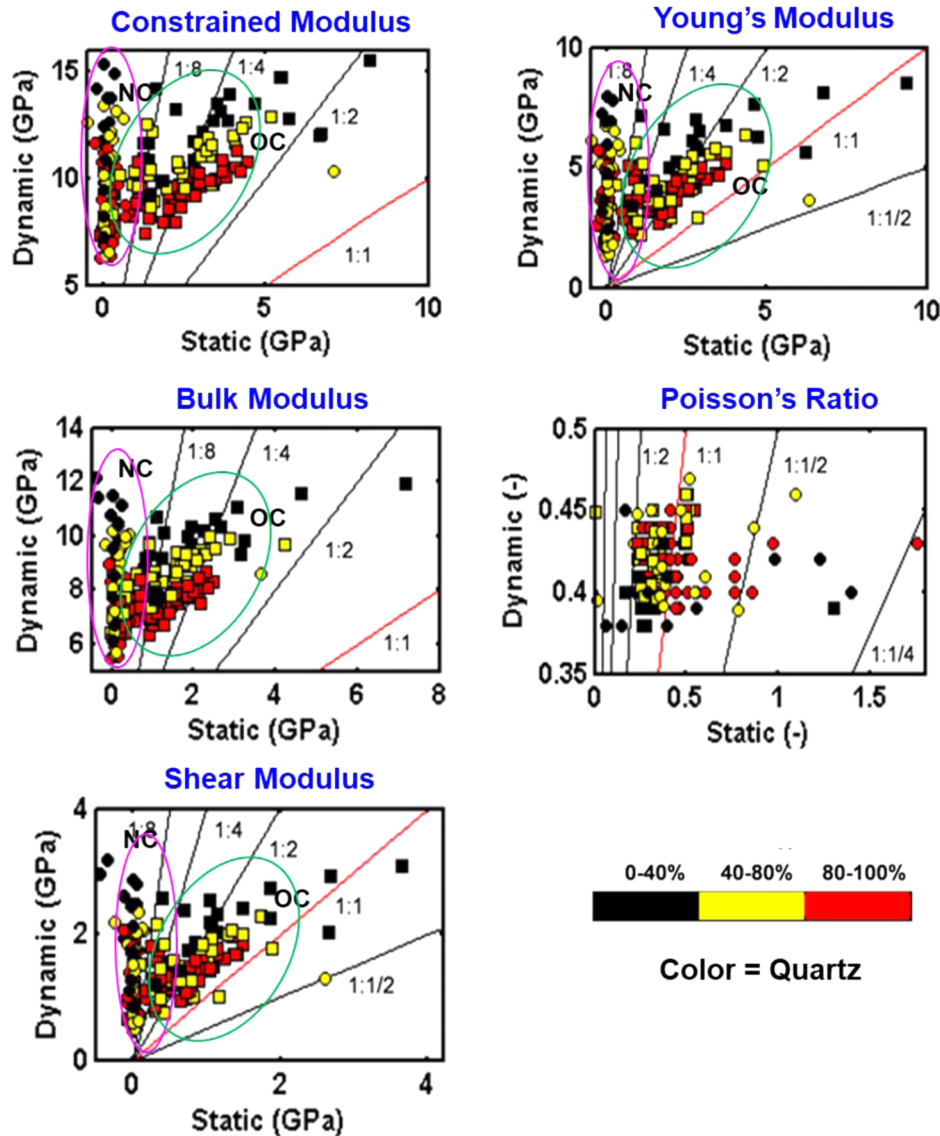


Figure 6 Relations between static and dynamic properties for all samples coloured by quartz content for all samples. Circles are normal consolidated (NC) sands, and squares are overconsolidated sands. The correspondences between 1:0.25 and 1:8 were projected on all static and dynamic elastic moduli relations. In all plots, for normal consolidation (circles) dynamic moduli are higher than static moduli as the data plotted beyond 1:8 correlation. Overconsolidated (OC) samples with high quartz show dynamic–static relation closer to 1:1 relationship compared to groups of samples with lower or medium quartz content. The OC (squares) have static and dynamic elastic relationship closer to 1:1 correspondence.

of pre-consolidation. Thus, the static moduli of the unloading/reloading sands correlate more closely with the dynamic elastic moduli. The static and dynamic relation of the constrained and bulk modulus exhibit a correlation between 1:3 and 1:8 correspondences. The shear modulus and the Young's modulus are closer to a one-to-one which observed to be between 1:1.5 and 1:8. Comparing between the influence of stress and sand compositions, the variations in all moduli are

affected by the mineral compositions as can be seen from Fig. 6. For example, the OC samples grouped as high quartz content is closer to a one-to-one relationship compared to the other two groups. This observation suggested that static modulus estimated from static–dynamic relations for OC sands can vary from 30% to 87% (1:1.5 to 1:8 correspondences) depending on mineral compositions (Fig. 6). On the other hand, the stress magnitude affects mainly the stiffness of the

sands; for example, the static–dynamic relationship between the Young’s moduli observed at a 1:2 correspondence still plot on the 1:2 line for all levels of stress magnitude (Fig. 5).

6 DISCUSSION

6.1 Horizontal stress development and stress path

Knowing the magnitude of the minimum horizontal stress is important for drilling operations in petroleum exploration and development which is imperative for safe drilling. Mud weight used to counteract subsurface pore pressure should not exceed the minimum horizontal stress to prevent drilling fluid losses into the formation through reopening of existing fractures or invasion into permeable formations. Therefore, predicting horizontal stress, especially in the area where there is no well control, through the relationship between the K_0 and effective stress can be useful.

Several plots of stress path (K_0 , i.e. Fig. 2b–d) show that K_0 under normal consolidated conditions (K_{0nc}) ranges between 0.45 and 0.58 while K_0 under overconsolidated (OC) conditions (K_{0oc}) starts from the K_{0nc} points and further increases to 1 as a function of overconsolidation ratio (OCR). Mayne and Kulhawy (1983) determine relationship between K_0 and OCR on the effect of stress history by compiling data from hundreds of different soils. The relation is expressed as

$$K_{0oc} = (1 - \sin \theta') \text{OCR}^{\sin \theta'} \quad (13)$$

The analysis of unloading stress path that linked between K_0 and OCR are built on Jaky’s simplified equation (Jaky 1948). For normally consolidated materials, $\text{OCR} = 1$, and equation (13) reduces to $K_{0oc} = (1 - \sin \theta') = K_{0nc}$. The θ is frictional angle. For example, if $\theta' = 30^\circ$, $K_{0nc} = 0.5$.

In the present study, the K_0 and OCR relationship exhibits two distinct trends separating between a group of high quartz samples and a group of low-medium quartz samples (Fig. 7). The best fit was performed in the form of the power function as in equation (13) on the two groups of samples and arrived at the following correlations:

For high quartz:

$$K_{0oc} = 0.53 \text{OCR}^{0.53} \quad (14)$$

For low to medium quartz:

$$K_{0oc} = 0.47 \text{OCR}^{0.47} \quad (15)$$

If the material is lacking internal friction angle information (θ'), above best fit functions can be used for a simplified estimation of K_0 if OCR is known.

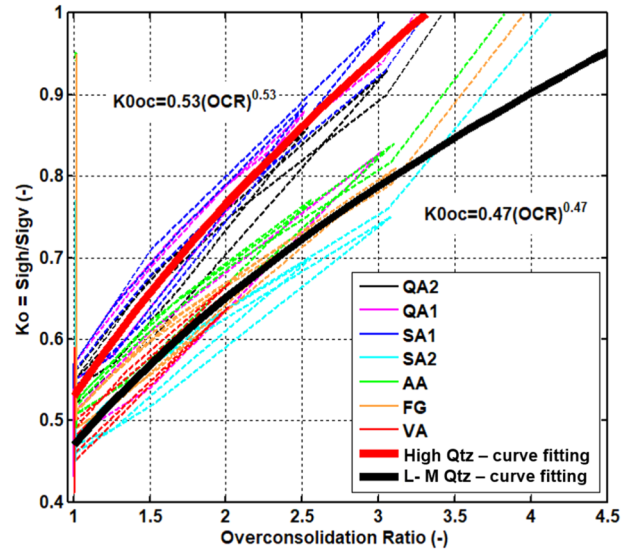


Figure 7 Polynomial best fit functions established for K_0 and overconsolidation ratio (OCR). Thin solid lines aligned across the whole range of K_0 (0.4–0.95) at $\text{OCR} = 1$ and dashed lines are measured data from all samples in this study. The data trends show a group of high quartz (red thick line) and low quartz samples (black thick line).

The effect of stress release as the reduction of vertical effective stress causes an increase in horizontal effective stress through the increase of K_0 value ($K_0 = \sigma'_h / \sigma'_v$). Therefore, this may have implications for safe drilling in uplifted region because the difference between horizontal stress minus pore pressure (assuming hydrostatic pore pressure) may be large (wide safely drilling window) as the horizontal stress is high due to the effect of overburden removal.

6.2 Dynamic and static elastic behaviour

The dynamic elastic moduli derived from wave propagation through ultrasonic measurement and static elastic moduli derived from deformation loading are different as previously reported (Figs 4–6). Several previous studies have explained potential causes of the difference (e.g. Jizba and Nur 1990; Fjær 1999; Wang 2000). One of which is the difference in strain amplitude between the two measurements (Martin and Haupt 1994). In the dynamic wave propagation experiment, the elastic strain amplitude is $<10^{-6}$ while static strain is typically $>10^{-2}$ (Wang 2000). Fjær (2009) also supported this assumption on his experiment on dry weak sandstone. Other plausible causes giving rise to the difference between static and dynamic moduli were summarized by Wang (2000) and Mavko *et al.* (2009). The suggested cause includes the effect

of pore pressure and testing conditions in open and closed systems. The dynamic elastic moduli derived from wave propagation usually denote an undrained or closed system and are influenced by the elastic properties of the pore fluid. This is in contrast to static moduli, where in the experiment, the pore pressure is kept constant, thereby representing a drained or open system. Bhuiyan *et al.* (2013) shows that by removing the effect of pore fluids through a Biot–Gassmann approach, static and dynamic moduli become comparable for sandstone.

The static–dynamic elastic moduli relation of overconsolidated (OC) sand condition in the present study is closer to a 1:1 relationship compared to the normal compacted sand condition (Figs 4–6). This shows that the sands that previously underwent OC or unloading deformed under smaller linear elastic strains while normal compacted sands deformed under significant larger nonlinear plastic strains. Therefore, the small elastic strain amplitude of static moduli of unloading is closer to the strain amplitude of dynamic moduli. As a result, the dynamic–static elastic moduli during unloading are nearly comparable, especially for Young’s and shear modulus. This phenomenon supports strain amplitude as plausible cause of the significant differences observed between static and dynamic properties in unconsolidated sands. This behaviour was also observed by Fjær (2009) on sandstones and Sone and Zoback (2013) on gas shales. Static and dynamic elastic moduli of unloading (or OC) can be appropriately compared with almost equal strain amplitudes and at identical physical properties of the solid rock skeleton. This implies that during the depletion and injection of a shallow unconsolidated reservoir experienced uplift (unloading) from overburden removal, approximating static modulus from dynamic modulus will be less difference in the magnitude as the relation is closer to one-to-one correspondence than the normally compacted reservoir.

7 CONCLUSION


Experimental mechanical compaction of sands integrating loading, unloading and reloading cycles confirms that stress release affects the rock physical properties and influences the seismic and mechanical properties. It is shown here that geomechanical parameters such as strain and stress are difference between normal compaction and overconsolidation (OC). Stress path (K_0) data differ between normal consolidated (NC) and OC sediments. The K_0 value of approximately 0.5 is found for most of the NC sands, but varies during unloading depending on mineral compositions and textural differences. The K_0 equation can be further simplified and can

be influenced by the material compositions. Acoustic velocity and geomechanical relation is also found to be the differences between two stress conditions. The static moduli of the OC sands are much higher than normal consolidated sands as the deformation is small (small strain). Dynamic–static elastic moduli relations more closely correlate for the OC stage compared to the normally consolidated stage. The experimental results presented herein are only valid for unconsolidated sands that have been compacted and unloaded/reloaded within the mechanical compaction domain. The results of the study have seismic-geomechanics applications for shallow reservoir sands where mechanical compaction is the dominant process.

ACKNOWLEDGEMENTS

We would like to thank the Norwegian Research Council (NFR) for funding the BarRock (Barents Sea Rock Properties) project under the program PETROMAKS (Programme for the Optimal Management of Petroleum Resources). We are also grateful to many NGI personnel, especially Toralv Berre, for their dedicated help with sample preparation, experimental setup and testing program.

ORCID

Sirikarn Narongsirikul 
<https://orcid.org/0000-0001-5242-4663>

REFERENCES

- Avseth P. and Lehocki I. 2016. Combining burial history and rock-physics modeling to constrain AVO analysis during exploration. *The Leading Edge* **35**, 528–534.
- Berre T. 2011. Triaxial testing of soft rocks. *Geotechnical Testing Journal* **34**, 61–75.
- Bhuiyan M.H., Holt R.M., Larsen I. and Stenebråten J. 2013. Static and dynamic behaviour of compacted sand and clay: comparison between measurements in triaxial and oedometric test systems. *Geophysical Prospecting* **61**, 329–340.
- Bhuiyan M.H., Kolstø M.I. and Holt R.M. 2011. Effects of stress and strain on wave velocities in compacted sand-kaolinite and kaolinite-smectite. 73rd EAGE Conference & Exhibition Incorporating SPE EUROPEC 2011, Extended Abstracts.
- Bjørlykke K. 2010. *Petroleum Geoscience: From Sedimentary Environments to Rock Physics*. Springer
- Bowers G.L. 1995. Pore pressure estimation from velocity data: accounting for overpressure mechanisms besides undercompaction. *Society of Petroleum Engineers* **10**, 89–95.
- Bowers G.L. and Katsube T.J. 2002. The role of shale pore-structure on the sensitivity of wireline logs to overpressure. In: *Pressure Regimes in Sedimentary Basins and their Prediction*, Vol. 76 (eds

- A.R. Huffman and G.L. Bowers), pp. 43–60. American Association of Petroleum Geologists.
- Casagrande A. 1936. The determination of the pre-consolidation load and its practical significance. *Proceedings of the International Conference on Soil Mechanics and Foundation Engineering* 3. pp. 60–64. Harvard University Cambridge.
- Chuhan F.A., Kjeldstad A., Bjørlykke K. and Høeg K. 2003. Experimental compression of loose sands: relevance to porosity reduction during burial in sedimentary basins. *Canadian Geotechnical Journal* 40, 995–1011.
- Dræge A., Duffaut K., Wiik T. and Hokstad K. 2014. Linking rock physics and basin history — Filling gaps between wells in frontier basins. *The Leading Edge* 33, 240–246.
- Dvorkin J. and Nur A. 1996. Elasticity of high-porosity sandstones: theory for two North Sea datasets. *Geophysics* 61, 1363–1370.
- Fawad M., Mondol N.H., Jahren J. and Bjørlykke K. 2011. Mechanical compaction and ultrasonic velocity of sands with different texture and mineralogical composition. *Geophysical Prospecting* 59, 697–720.
- Fjær E. 1999. Static and dynamic moduli of weak sandstones. *The 37th U.S. Symposium on Rock Mechanics, ARMA-99-0675*, Vail, CO, 7–9 June. American Rock Mechanics Association.
- Fjær E. 2009. Static and dynamic moduli of a weak sandstone. *Geophysics* 74, 1942–2156.
- Geertsma J. 1973. Land subsidence above compacting oil and gas reservoirs. *Journal of Petroleum Technology* 25, 734–744.
- Grande L., Mondol N.H. and Berre T.K. 2011. Horizontal stress development in fine-grained sediments and mudstones during compaction and uplift. 73rd EAGE Conference & Exhibition incorporating SPE EUROPEC, Vienna, Austria, 23–26 May 2011, Extended Abstracts.
- Hatchell P. and Bourne S. 2005. Rock under strain: Strain-induced time-lapse time shifts are observed for depleting reservoirs. *The Leading Edge* 24, 1222–1225.
- Herwanger J.V. and Horne S.A. 2009. Linking reservoir geomechanics and time-lapse seismics: predicting anisotropic velocity changes and seismic attributes. *Geophysics* 74, 13–33.
- Holt R.M. 1994. *Effects of coring on petrophysical measurements*. International Symposium of the Society of Core Analysts Paper SCA9407.
- Holt R.M. 1999. *Laboratory acoustic measurements for reservoir characterization: consequences of core alteration*. International Symposium of the Society of Core Analysts Paper SCA9926.
- Holt R.M., Bauer A., Bakk A. and Szewczyk D. 2016. Stress-path dependence of ultrasonic and seismic velocities in shale, SEG Technical Program Expanded Abstracts: 3159–3163.
- Holt R.M., Nes O-M. and Fjær E. 2005. In-situ stress dependence of wave velocities in reservoir and overburden rocks. *The Leading Edge* 24, 1268–1274.
- Jaky J. 1948. Pressure in silos. *Proceedings of the 2nd International Conference on SMGE*. pp. 103–109.
- Jizba D. and Nur A. 1990. Static and dynamic moduli of tight gas sandstones and their relation to formation properties. SPWLA 31st Annual Logging Symposium, Lafayette, LA, 24–27 June.
- Martin R.J. and Haupt R.W. 1994. *Static and Dynamic Elastic Moduli in Granite: The Effect of Strain Amplitude*. American Rock Mechanics Association.
- Mavko G., Mukerji T. and Dvorkin J. 2009. *The Rock Physics Handbook: Tools for Seismic Analysis in Porous Media*. Cambridge University Press.
- Mayne P.W. and Kulhawy F.H. 1983. K-OCR relationships in soil. *Journal of the Geotechnical Engineering Division* 20, 851–869.
- Mondol N.H., Avseth P., Fawad M. and Smith T. 2010. Vs prediction in unconsolidated sands: physical and Geological controls on shear wave velocity. 72nd EAGE meeting, Expanded Abstracts, 351.
- Narongsirikul S., Mondol N.H. and Jahren J. 2019a. Acoustic and petrophysical properties of mechanically compacted overconsolidated sands: part 1 – Experimental results. *Geophysical Prospecting* 67, 804–824.
- Narongsirikul S., Mondol N.H. and Jahren J. 2019b. Acoustic and petrophysical properties of mechanically compacted overconsolidated sands: part 2 – Rock physics modelling and applications. *Geophysical Prospecting* 67, 114–127.
- Nygård R., Gutierrez M., Høeg K. and Bjørlykke K. 2004. Influence of burial history on microstructure and compaction behavior of Kimmeridge clay. *Petroleum Geoscience* 10, 259–270.
- Pender M.J. 1978. A model for the behaviour of overconsolidated soil. *Geotechnique* 28, 1–25.
- Petterson Ø. 2007. Sandstone compaction, grain packing and critical state theory. *Petroleum Geoscience* 13, 63–67.
- Rickett J., Duranti L., Hudson T., Regel B. and Hodgson N. 2007. 4-D time strain and the seismic signature of geomechanical compaction at Genesis. *The Leading Edge* 26, 644–647.
- Røste T., Stovas A. and Landro M. 2005. Estimation of layer thickness and velocity changes using 4D prestack seismic data. 67th EAGE Annual Conference and Exhibition, Extended Abstracts.
- Sone H. and Zoback M.D. 2013. Mechanical properties of shale-gas reservoir rocks — Part 1: static and dynamic elastic properties and anisotropy. *Geophysics* 78, D381–D392.
- Tao G., King M.S. and Nabi-Bidhendi M. 1995. Ultrasonic wave propagation in dry and brine-saturated sandstones as a function of effective stress: laboratory measurements and modelling. *Geophysical Prospecting* 42, 299–328.
- Terzaghi K. 1943. *Theoretical Soil Mechanics*. John Wiley & Sons.
- Wang Z. 2000. Dynamic versus static elastic properties of reservoir rocks. In: *Seismic and Acoustic Velocities in Reservoir Rocks*, Vol. 3 (eds Z. Wang, and A. Nur), pp. 531–539. Society of Exploration Geophysicists.
- Yin H. 1992. *Acoustic velocity and attenuation of rocks: Isotropy, intrinsic anisotropy and stress induced anisotropy*. PhD thesis, Stanford University, Stanford, CA.
- Zimmer M.A., Prasad M., Mavko G. and Nur A. 2007. Seismic velocities of unconsolidated sands: Part 1 – Pressure trends from 0.1 to 20 MPa. *Geophysics* 72, 1–13.